Dynamic coordination of the perirhinal cortical neurons supports coherent representations between task epochs

Tomoya Ohnuki *, Yuma Osako, Hiroyuki Manabe, Yoshio Sakurai & Junya Hirokawa *

Laboratory of Neural Information, Graduate School of Brain Science, Doshisha University, 1-3 Tatara Miyakodani, Kyotanabe, Kyoto, 610-0394, Japan.

*Correspondence and requests for materials should be addressed to T.O. (kdp1003@mail4.doshisha.ac.jp) and J.H. (jhirokaw@mail.doshisha.ac.jp).

Abstract

Cortical neurons show distinct firing patterns across multiple task-epochs characterized by distinct computational aspects. Recent studies suggest that such distinct patterns underly dynamic population code achieving computational flexibility, whereas neurons in some cortical areas often show coherent firing patterns across epochs. To understand how such coherent single-neuron code contribute to dynamic population code, we analyzed neural responses in the perirhinal cortex (PRC) during cue and reward epochs of a two-alternative forced-choice task. We found that the PRC neurons often encoded the opposite choice-directions between those epochs. By using principal component analysis as population-level analysis, we identified neural subspaces associated with each epoch, which reflected coordinated patterns across the neurons. The cue and reward epochs shared neural dimensions where the choice directions were consistently discriminated. Interestingly, those dimensions were supported by dynamically changing contributions of individual neurons. These results indicated heterogeneity of coherent single-neuron responses in their

contribution to population code.

Introduction

Individual neurons across cortical areas show temporally flexible responses to multiple task-epochs characterized by different computational aspects, such as cue, action, and reward[1–3]. Recent studies have indicated that such diverse single-neuron responses are only interpretable in terms of their contribution to population dynamics which flexibly realize different computations, particularly in association and motor cortices[4–9]. These studies highlight the complex changes occurring in neural responses across epochs of a given task, which can provide orthogonal neural subspaces for independent computations. In contrast, individual neurons in many cortical areas have been shown to often encode relevant information across multiple epochs (Anterior cingulate cortex[10], Insular cortex[11], Motor cortex[12], Orbitofrontal cortex[13–15], and Perirhinal cortex[16]), suggesting their ability to support coherent representations through different task-epochs. Because of

the differences in the forms of explanation in these studies (that is, population or single-neuron level), how coherent representations carried by individual neurons can be reconciled with dynamically changing population structure has not been well investigated.

In the present study, we explored the neural responses in the perirhinal cortex (PRC), which has been implicated in associative memory [17–22]. This region receives sensory inputs from almost all modalities, reward-related signals from the amygdala and contextual information from the prefrontal cortex, entorhinal cortex and hippocampus[23–25]. Recent studies have shown that the PRC neurons modulate their sustained responses to visual cues as a function of time contexts[26–27]. It has also been shown that many neurons in the PRC change their tuning profiles between cue and choice-response epochs in a complex manner[14]. These results strongly suggest the capacity of the PRC neural population to employ both population dynamics and coherent representations through multiple task-epochs.

To investigate how the PRC shows coherent single-neuron code and dynamic population code across different epochs, we employed a standard two-alternative forced-choice task and analyzed neural responses in two

67 epochs, where different computations are demanded: making predictions
68 about the outcome of choices (cue epoch) and reinforcing the choices (reward
69 epoch). By taking advantage of the interleaved visual and olfactory cue
70 stimuli, which allowed us to evaluate modality-independent encodings, we
71 analyzed dynamic population encodings related to different choices during
72 those epochs in relation to single-neuron level selectivity.
73
74
75 **Results**
76
77 **Neurons in the PRC encode choice directions during a two-alternative**
78 **forced-choice task.** We trained rats to perform a two-alternative forced-
79 choice task where they chose a target port (left/right) associated with a
80 presented cue to obtain reward (**Fig. 1a–b**). The task performance was of a
81 similar level regardless of the cue modality (mean correct rate in visual
82 trials = 95.6 ± 5.5%; olfactory trials = 92.3 ± 4.3%). We recorded spiking
83 activities from the left PRC (n = 207 neurons) during the task performance
84 (37 sessions in five rats).

85 As shown in **Fig. 1c**, the PRC neurons typically showed distinct temporal
86 firing patterns in left and right trials. To characterize how the PRC was
87 activated by different trial conditions, we compared firing pattens among
88 different cue-modalities and choices across all the recorded neurons. The
89 neurons were sorted by their peak firing rates in visually-cued left choice
90 trials (top left in **Fig. 1d**). As consistent with previous studies in other brain
91 regions[28–33], the peak responses of the PRC neurons tiled the duration of a
92 trial. The response patterns across the neurons were well preserved
93 between the cue modalities but much less so between the choice directions
94 (comparison between the top and bottom in **Fig. 1d**). Conversely, the
95 neurons frequently showed different response pattens between the choice
96 directions (comparison between the left and right in **Fig. 1d**). We found that
97 the majority of the neurons showed more strongly correlated response
98 patterns between different modalities than between different choice
99 directions (two-sided Wilcoxon signed-rank test; $P = 1.1864 \times 10^{-24}$; **Fig. 1e**).
100 These results suggest that firings of the PRC neurons are more sensitive to
101 the animals' choice behavior than cue information.
102 We thus quantified selective responses of the individual neurons to the

103 different choice-directions by using ROC analysis. We defined "choice-
104 direction selectivity" broadly as signals reflecting a chosen direction in each
105 trial. The individual PRC neurons encoded the choice directions at different
106 time points in a trial (**Fig. 2a** for visual trials; **Supplementary Fig.1** for
107 olfactory trials). In addition, each neuron often showed such encodings at
108 the time points other than its peak selectivity, suggesting that the
109 individual neurons flexibly respond to multiple epochs of the task. We found
110 two epochs where the choice-direction selectivity in both modalities reaches
111 its peak (**Fig. 2b**), the cue epoch (−400 to 0 ms before withdrawal from the
112 central port) and reward epoch (200 to 600 ms after choice). Many neurons
113 encoded the choice-direction information during these epochs (**Fig. 2c**;
114 51.21% and 70.53% of the neurons showed significant selectivity in the cue
115 and reward epochs, respectively). We observed a slight bias toward
116 ipsilateral choice in the cue epoch (two-sided sign test; mean visual choice-
117 direction selectivity = 0.006 ± 0.124, P = 0.8894; mean olfactory choice-
118 direction selectivity = 0.0250 ± 0.102, $P = 5.104 \times 10^{-4}$) but no bias in the
119 reward epoch (two-sided sign test; mean visual choice-direction selectivity =
120 −0.026 ± 0.154, P = 0.2109; mean olfactory choice-direction selectivity =

121 -0.021 ± 0.154, $P = 0.3305$). The choice-direction selectivity was highly

122 consistent across the cue modalities during both epochs ($r = 0.593$, $P =$

123 5.1803×10^{-21} for the cue epoch; $r = 0.858$, $P = 2.8367 \times 10^{-61}$ for the reward

124 epoch; **Fig. 2c**), and the PRC neurons were not tightly clustered as a choice-

125 direction selective subpopulation and the others but rather showed graded

126 selectivity as reported in other cortical areas[7, 34]. The neurons which showed

127 significant selectivity across both modalities were sparser in the cue epoch

128 (26% of selective neurons) than the reward epoch (48% of selective neurons),

129 but we found that the neurons classified as non-selective during the cue

130 epoch (48.79%, 101 of 207 neurons) showed moderate correlation between

131 the cue modalities ($r = 0.357$, $P = 2.5054 \times 10^{-4}$; inset of **Fig. 2c**). This

132 suggested even such neurons might convey a fraction of the choice-direction

133 information. Altogether, these results suggest that sensory inputs from

134 different modalities evoke similar response patterns across the PRC

135 neurons according to learned cue-target associative relationships.

136 A potential caveat in this conclusion, however, is that the choice-direction

137 selectivity in the PRC can be attributed to some fundamental behavioral or

138 contextual variables such as body posture, non-orienting movements, and

spatial view[30, 35–39]. To evaluate the possible influence of those fundamental variables, we performed two control experiments. First, we monitored head angles of the animals ($n = 2$) during neural recordings (**Supplementary Fig. 2a–c**) using a head-mounted accelerometer[40]. To quantify the influence of body posture and view angle on the PRC neural responses ($n = 105$), we compared prediction performance between linear-regression models with choice and x-axis (interaural axis) head angle by computing correlation between the neural responses and the model prediction across trials (**Supplementary Fig. 2d**). The performance of the model with choice was higher than the model with x-axis head angle in both of the cue and reward epochs by 4.28% ± 10.98% (m.a.d) and by 32.07% ± 34.8% (m.a.d), respectively. We found that responses of the majority of the PRC neurons was better explained by the choice than the x-axis head angle (two-sided sign test; cue epoch, $P = 0.0192$; reward epoch, $P = 1.3653\times10^{-7}$). Second, a delay period was inserted between the choice onset and the reward onset to dissociate the influence of anticipatory licking behavior[41] and spatial view (position) from the choice-direction selectivity in the reward epoch. We found that many of the neurons (69.52%, 73 of 105 neurons) encoded choice-

direction after the onset of the reward (0 to 400 ms after reward onset) in accordance with the reward-epoch responses shown in **Fig. 2c**. The majority of these selective neurons (71.23%, 52 of 73 neurons) showed stronger selectivity after the onset of the reward than during the reward delay period (two-sided sign test; median difference in the magnitude of selectivity = 0.08, $P = 3.7134\times10^{-4}$; **Supplementary Fig. 2e**). Although the other neurons (28.77%; 21 of 73 neurons) showed stronger selectivity during the reward-delay period than after the reward onset, the size of such bias (that is, difference in magnitude between these periods) was relatively small (0.058 ± 0.0609; $n = 21$ neurons) as compared to the bias to the reward onset (0.1586 ± 0.1217; $n = 52$ neurons). Taken together, these results suggest that fundamental variables such as body posture, non-orienting movements, and spatial view themselves are not major factors for the choice-direction encodings in the PRC.

Dynamic temporal encoding patterns in the PRC. Thus far, we showed that the PRC neurons encoded the choice directions across the different cue modalities and that such signals were apparent at multiple epochs of the

175 task (**Fig. 2** and **Supplementary Fig.2**). Given the reduced correlation of
176 temporal response patterns between the different choices (**Fig. 1d–e**), it is
177 possible that the individual neurons flexibly tuned to different choices at
178 different time-points of the trial duration. To characterize how each neuron
179 represented the choice directions over the trial duration, we classified the
180 neurons into two groups based on their peak selectivity: left-selective and
181 right-selective neurons. As shown in **Fig. 3a**, we found similar numbers of
182 selective neurons for both choice-directions. As expected, individual neurons
183 showed selectivity to the opposite choice direction in time points other than
184 their peak responses. Remarkably, when we sorted these neurons by their
185 peak responses to the opposite choice (that is, left-selective neurons by right
186 peaks and right-selective neurons by left peaks), response patterns nearly
187 tiling the entire trial duration appeared (**Fig. 3b**). These results suggested
188 flexible engagements of individual neurons for different choice-directions
189 rather than recruitment of distinct subpopulations for each choice-direction.
190 We next sought to understand how such dynamic neural encoding
191 patterns in the PRC appear and evolve through the trial duration as a
192 population. A time-resolved pattern analysis[42] (**Methods**) was performed to

visualize temporal evolution of the choice-direction encoding patterns across the PRC neurons ($n = 207$). Given the overall correlation of the choice-direction selectivity between the cue-modalities during the epochs where such encodings peak (**Fig. 2 b–c**), we focused on modality-independent encoding patterns (for comparison between the visual and olfactory trials, see **Supplementary Fig. 3**). The population response pattern evolved with two time-stable states (**Fig. 4a**). An encoding pattern was sustained during the presentation of the cue and was followed by a transient pattern during the movements towards the target ports. Soon after the rats chose a target port, the encoding pattern settled again into a stable state. To test for reliability of such encodings, we computed the mean performance of the classifier during the cue and reward epochs and compared them with a baseline epoch (−400 to 0 ms before the cue onset). As shown in **Fig. 4b**, the choice directions were decoded during both epochs above chance level (cue epoch: $P \approx 0.002$; reward epoch: $P < 0.001$). Importantly, the encoding patterns were substantially inverted between the cue and reward epochs (scatter plots in **Fig. 4a**). The mean classification performance across those epochs revealed reliably inverted encoding patterns ($P < 0.001$; **Fig. 4c**). It is

211 noteworthy that the inverted state was time-stable (**Fig. 4a**). This indicates
212 that the time-varying encodings of the choice directions which we found in
213 the previous section (**Fig. 3b**) are explicitly aligned to between the cue and
214 reward epochs. In other word, the inverted encodings might be a form of
215 coherent representations across different epochs of a given task, which is
216 mediated by the individual PRC neurons.

217 However, it is still possible that the inverted encoding patterns were due
218 to the reversal of orienting movements between the cue and reward epochs.
219 To directly test this, we analyzed neural responses around the time when
220 the animals left the target ports in preparation to the next trials
221 (**Supplementary Fig. 4**): the pre-return (−400 to 0 ms before the choice offset)
222 and post-return epochs (0 to 400 ms after the choice offset). These epochs
223 did not show the equivalent level of inverted patterns from the cue epoch
224 (cue × pre-return epochs: $P \approx 0.016$; cue × post-return epochs: $P \approx 0.1858$;
225 comparison between cue×reward epochs and cue×pre-return epochs: $P \approx$
226 0.023; **Fig. 4c**) despite the fact that the choice-direction information was
227 robustly represented during both pre-return and post-return epochs ($P <$
228 0.001; **Fig. 4d**). These results indicated little influence of orienting

movements on the dynamic choice-direction encoding patterns.

We also asked whether the behavioral performance affect neural responses by performing the pattern classification analysis with correct visual and erroneous olfactory trials (n = 119 neurons with sufficient number of erroneous trials; **Fig. 4e**). As shown in **Fig. 4f** the mean classification performance during both epochs was chance level in erroneous trials (error cue: $P \approx 0.1389$; error reward: $P \approx 0.1349$). Meanwhile, in correct trials, the mean classification performance was above chance for the reward epoch and marginally significant for the cue epoch (correct cue: $P \approx 0.0729$; correct reward: $P < 0.001$). We tested whether the classification performance during each epoch decreased from the correct trials to erroneous trials and found significant reduction only in the reward epoch (cue: $P \approx 0.5385$; reward: $P < 0.001$). These results indicate dynamic recruitment of the PRC neurons during the different epochs, which might flexibly support different computational demands in each epoch.

Analysis for population encoding structure in relation to single-neuron representations. To investigate how such coherent response patterns

appeared and worked under the entire population structure, we identified neural subspaces for the cue and reward epochs by performing principal component analysis (PCA). Since our focus was to compare population response patterns between the different epochs, PCA was applied to time-averaged cue-epoch and reward-epoch responses across conditions (that is, PCA on neurons × conditions matrix for each epoch) [43–44]. This allowed us to clarify the population-encoding structure derived from the cue-epoch responses and reward-epoch responses and directly investigate interrelationship between them. We projected the cue-epoch and reward-epoch responses onto the first two dimensions of the cue-epoch and reward-epoch subspaces (**Fig. 5a** and **Supplementary Fig. 5a**). The different choices and cue modalities were clearly separated when we projected the neural responses onto the corresponding neural subspaces (**Fig. 5a,** cue epoch in upper left; reward epoch in bottom right). Although we observed highly correlated choice-direction selectivity between the visual and olfactory cues (**Fig. 2c**), modality information was evident in these plots. We quantified separation among the four different conditions in those plots by comparing the average distance among responses under different conditions (across-

condition distance) with the average distance among responses under the same conditions (within-condition distance). The former distance indicates discriminability of the different conditions and the latter indicates variability of the population responses within each condition. The results revealed that the across-condition distance was significantly larger than within-condition distance in both projections, indicating reliable encodings of the different conditions during both epochs ($P < 0.001$; **Fig. 5b** and **Methods**). We also determined whether these neural subspaces depended on the entire neural population or on only a fraction of the neurons. We found that neural weights were highly distributed across the neurons (**Fig. 5d** and **Supplementary Fig. 5b**) with no neurons showing zero weight. This suggest that these subspaces reliably reflect coordinated response patterns across the PRC neurons. To directly investigate the relationship between the cue-epoch and reward-epoch responses, we projected the population responses onto interchanged neural subspaces (that is, the cue-epoch responses onto the reward-epoch subspace and the reward-epoch responses onto the cue-epoch subspace)[4,5,8]. The results showed that the choice directions but not the cue modalities were separable through the epochs (**Fig. 5a**, cue-epoch

283 responses onto reward-epoch subspace in bottom left; reward-epoch
284 responses onto cue-epoch subspace in upper right). For those interchanged
285 projections, we also quantified separations among different conditions by
286 the same method as the corresponding projections. As shown in **Fig. 5c,** in
287 both subspaces, we found cluster separations above chance (reward-epoch
288 responses in cue-epoch subspace: $P < 0.001$; cue-epoch responses in reward-
289 epoch subspace: $P \approx 0.003$), revealing that the choice-direction information
290 was reliably sustained between those different epochs. We also projected the
291 neural responses during the baseline epoch onto the same neural subspaces
292 as negative controls (**Supplementary Fig. 5c**). This analysis revealed no
293 significant cluster separations ($P \approx 1$ for cue-epoch subspace; $P \approx 1$ for
294 reward-epoch subspace; **Fig. 5c**), indicating no reliable encodings of the task
295 information. We then tested whether the temporal response patterns of the
296 individual neurons contributed to the observed discriminability by
297 projecting randomly shuffled data where the temporal response patterns of
298 the individual neurons were collapsed (**Supplementary Fig. 5d**). The results
299 showed no significant separations ($P \approx 1$ for shuffled reward-epoch
300 responses in cue-epoch subspace; $P \approx 0.99$ for shuffled cue-epoch responses

in reward-epoch subspace; **Fig. 5c**), suggesting that the coherence between the cue and reward epochs at the single-neuron level was critical for the discriminability observed at the population level.

It might be possible that only a handful of neurons had strongly contributed to both cue-epoch and reward-epoch subspaces, thus resulting in the shared neural dimensions (that is, the first dimensions which consistently discriminated the choice directions) shown in **Fig. 5a**. However, this was not the case. As shown in **Fig. 5e**, the plot of the values of neural weights in the first dimensions of the cue-epoch and reward-epoch subspaces showed neither explicit clusters nor a tight correlation but rather exhibited a continuous distribution with a moderate correlation ($r = 0.33$, $P = 1.51\times10^{-6}$). This suggests that many neurons dynamically changed their contribution to the shared dimensions across the epochs, while a degree of temporal coherence supporting those shared dimensions were maintained at the population level. Diverse relationships of neural weights of the cue and reward epochs were observed even among neurons with significant choice-direction selectivity (computed using ROC analysis in **Fig. 2c**) across the epochs (blue points in **Fig. 5e**). This result indicated heterogeneity of

319 temporally coherent single-neuron responses in their contribution to the
320 entire population structure. In other words, each of those neurons might
321 play unique role in population encodings under different computations.
322 To further establish population-level encoding[7, 34, 45–46] in the PRC, we
323 directly examined distribution of choice-direction information over
324 individual neurons. We asked what fraction of the neurons is necessary to
325 achieve choice-direction discriminability (that is, across-condition distance
326 for different choice directions on the first dimension of a given epoch) which
327 is equivalent to the entire population (**Methods**). The number of neurons
328 incorporated were gradually increased, beginning with ones with the
329 highest magnitude of the weighting values on the first dimension of the cue
330 or reward epoch (**Fig. 5f**). As expected from the shape of the distribution in
331 **Fig. 5d**, when the neurons were sorted by the cue-epoch weights, the choice-
332 direction discriminability in the cue subspace steeply increased with the
333 incorporation of neurons (left in **Fig. 5f**). However, the top 76.33% of the
334 neurons was necessary to achieve the discriminability as high as the entire
335 population. Similarly, when the neurons were sorted by the reward-epoch
336 weights, the discriminability in the reward subspace reached as high as the

337 full population after including 87.44% of the neurons (right in **Fig. 5f**). These
338 results support population-level representations in which information is
339 distributed across a number of individual neurons in the PRC. On the other
340 hand, the choice-direction discriminability more gradually increased for the
341 epochs to which the orders of neurons were not aligned (**Fig. 5f**),
342 highlighting the dynamic changes in the neural weights between the epochs
343 observed in **Fig. 5e**. We found that nearly all the neurons were necessary to
344 achieve the discriminability as high as the full population (neurons sorted
345 by cue-epoch weights, 100%; neurons sorted by reward-epoch weights,
346 98.55%), indicating that the choice-direction representations across the two
347 epochs were distributed widely over the entire population. However, the
348 mean discriminability in the epochs in which the neurons were indirectly
349 sorted more steeply increased than the linear increase which is expected
350 when the neurons were added in a random order (Kolmogorov-Smirnov test;
351 cue epoch, $P = 2.4985\times10^{-11}$; reward epoch $P = 0.0045$). As shown in **Fig. 5f**,
352 by incorporating a small subset of the neurons (~10%), those curves
353 deviated from the linear increase and the deviation was sustained through
354 the almost all the parts of the curves. Therefore, the choice-direction

355 information in the cue and reward epochs was highly distributed across the
356 neurons, but its coherence was reliably sustained at the population level.
357
358 **Efficient encoding of choice directions and different task-epochs by the PRC**
359 **population.** As shown in **Fig. 5a**, the population response patterns
360 representing the choice directions were substantially inverted when we
361 compared the cue-epoch responses and reward-epoch responses in the same
362 neural subspace (comparison between horizontally arranged plots in **Fig.**
363 **5a**). In contrast, when the population responses from one of these epochs
364 were projected onto the cue-epoch and reward-epoch subspaces (comparison
365 between vertically arranged plots in **Fig. 5a**), the relative positions of the
366 different choice-directions were preserved, indicating that the directions
367 (that is, signs) of the first dimensions were consistent. Therefore, these
368 results suggested that information of the different epochs was also
369 represented in the shared dimensions by flexible changes in the
370 representational geometry. The inverted geometry was consistent with the
371 dominant temporal response pattern observed in **Fig. 4a**. To test reliability
372 of the temporal inversions, in each subspace, we computed the average

distance between population responses under the same conditions in the different epochs (for example, distance from cue-epoch responses to reward-epoch responses in the cue subspace) (**Methods**). We compared those distances with average distance from one of those epochs to the baseline epoch (for example, distance from cue-epoch responses to baseline-epoch responses in the cue subspace), which is equivalent to chance-level cluster shifts caused by the absence of task representations (that is, overlapped clusters at near zero in **Supplementary Fig. 5c**). Therefore, if the representational patterns are reliably inverted between the cue and reward epochs, then the temporal shift distances between those epochs should be significantly larger than the chance-level shift distances. As shown in **Fig. 5g**, the results showed larger task-epoch dependent shifts of the representational patterns than expected by chance ($P \approx 0.002$ for cue-epoch subspace; $P \approx 0.009$ for reward-epoch subspace). The discriminability was diminished when the temporal patterns of individual neural responses were collapsed by data shuffling ($P \approx 1$ for shuffled reward-epoch responses in cue-epoch subspace; $P \approx 0.9021$ for shuffled cue-epoch responses in reward-epoch subspace). These results suggested that the coherent response

391 patterns at the individual neurons mediated flexible changes for task-epoch
392 representations. We next asked how these flexible encodings for the cue and
393 reward epochs (**Fig. 5g**) were related to the coherent choice-direction
394 encodings across these epochs (**Fig. 5c**). We projected the PRC population
395 responses onto the two axes capturing variances of those variables
396 (temporal coherence index and temporal shift index in **Fig. 5h**; **Methods**). We
397 found that variability of the population responses across subsets of trials
398 were clearly aligned to the line that maximized both indices (dashed line in
399 **Fig. 5h**), suggesting that the PRC population specifically tuned to support
400 both coherence and dynamics of neural representation between the epochs.
401 Transition of the population response between the cue and reward epoch
402 resulted in a high correlation between the two indices ($r = 0.629$, $P =$
403 2.8077×10^{-111}), but the correlation was absent in transition between the
404 baseline epoch and the cue or reward epochs ($r = -0.018$, $P = 0.5699$).
405 Importantly, the correlation depended on the temporal response patterns in
406 the individual neurons ($r = -0.088$, $P = 0.0055$ for shuffled responses),
407 suggesting that coherent single-neuron encodings were critical to efficiently
408 enhance coherence and dynamics of the neural representation. Taken

together, these findings indicated that the PRC population reconciles coherent representations of choice directions with dynamic representations for different epochs via temporally flexible but structured neural responses (that is, inverted selectivity between epochs).

Discussion

We investigated how coherent single-neuron representations across different epochs can be reconciled with temporal dynamics of population structure. Individual neurons in the PRC modulated their firings according to choice directions in each trial, and many neurons inverted such selectivity between the cue and reward epochs. Despite the structured temporal response patterns, we found dynamic reorganization of the population encoding structure between the different epochs (that is, neural subspaces supported by different coordination patterns across neurons). Yet, we also found shared neural dimensions between the cue and reward epochs, where the choice-direction information was consistently represented throughout the epochs.

427 Those dimensions depended on the coherent temporal patterns of the single-
428 neuron responses. These findings indicated that the temporally structured
429 single-neuron responses worked as a dynamic population structure,
430 supporting coherent representations throughout epochs of a given task.
431 It is recently suggested that choice-related encodings observed in higher-
432 order cortical areas are not necessarily abstract signals but rather
433 parsimoniously explained by combination of fundamental behavioral and
434 contextual variables such as a specific spatial position and head angle[36].
435 Additionally, a recent study in rats revealed that neurons in the lateral
436 entorhinal cortex are sensitive to subtle changes of egocentric view[37]. In
437 contrast to these results, our analysis revealed that the choice directions
438 were a better predictor for the individual PRC neural responses than other
439 major variables previously noted, namely, body posture, non-orienting
440 movements and spatial view (**Supplementary Fig. 2**). Although those
441 individual factors could influence on the PRC responses, they were not
442 unique to evoke the PRC responses. Thus, we conclude that the choice-
443 direction encodings in the PRC is not derived from these single behavioral
444 variables but rather an abstract signal integrating various computations

445 related to the choice at a given epoch.

446 How does the nature of the choice-direction encodings differ between the
447 cue and reward epochs? We further characterized those encodings by
448 comparing between the correct and erroneous trials for each epoch (**Fig. 4e–**
449 **f**). In the cue epoch, we did not find significant difference between choice-
450 direction encodings in the correct and erroneous trials. Given that those
451 neural responses are better explained by the choice directions than by head
452 angles (**Supplementary Fig. 2d**), the cue-epoch responses might reflect
453 internal signals such as decision or motor preparation driven by reward
454 expectation[16, 47–50]. Contrary, in the reward epoch, the choice-direction
455 encodings significantly decreased in erroneous trials. The reduction suggest
456 that the presence of reward was necessary to elicit those responses.
457 Furthermore, the reward-epoch responses were temporally locked to the
458 onset of reward and were not elicited by spatial position, view angle, reward
459 expectation or combinations of them (**Supplementary Fig. 2d–e**). Therefore,
460 those responses might convey reward signals in conjunction with choice
461 directions. Those distinct choice-related representations were not expected
462 by previous studies, most of which highlights perceptual and mnemonic

463 representations in the PRC[18–22, 51–54]. However, a recent lesion study
464 suggests that the PRC is also involved in value-based decision making[55]. In
465 light of widespread anatomical connections of the PRC[23–25], it is possible
466 that this region carries diverse information besides perceptual and
467 mnemonic signals depending on neural computation required for the task[56].
468 The above results emphasize different neural computations reflected in
469 choice-direction selectivity in each of the cue and reward epochs. In spite of
470 the explicit difference, the PRC neurons often showed choice-direction
471 encodings in both epochs, suggesting that they support associative
472 representations of choice and its outcome. This agrees with a traditional
473 view, which holds that the PRC supports associative memory[14,18–22]. Several
474 studies showed that temporally sustained responses were prevalent in the
475 PRC[16, 22–27]. Such sustained responses were found in studies focusing on
476 neural responses during cue and memory epochs and were considered to
477 serve as stable representations of targeted information across time epochs,
478 which enable typical functions of the PRC including recognition memory[57].
479 Our finding of the inverted response patterns was not predicted by those
480 previous studies but suggested its advantage in supporting both temporal

481 coherence and flexibility of neural representations. By using the
482 dimensionality reduction technique, we showed that the inverted encoding
483 patterns of the PRC population mediated representations of the different
484 epochs as well as consistent discriminability of the different choice-
485 directions (**Fig. 5c, g**). Moreover, an important finding in our study is that
486 the discriminability of the choice directions and task epochs was highly
487 correlated (**Fig. 5h**). These results not only indicate dynamics of the PRC
488 responses, which was underestimated in previous studies, but suggest an
489 encoding strategy in the PRC efficiently enhanced discriminability of
490 information from multiple sources across task epochs.

491 It is worth mentioning that values of neural weights of the individual
492 neurons varied between the cue and reward epochs. In spite of the
493 heterogeneity in individual neurons, at the population-level, the neural
494 weights were moderately correlated between the epochs, resulting in the
495 coherent choice-direction representations (**Fig. 5e–f**). Heterogeneous
496 response properties across individual neurons are often observed in high-
497 order cortical areas[29, 31, 38, 58–60] and are considered to increase the number of
498 dimensions can be represented by a neural population[8, 61–64]. In some cases,

neurons exhibit a high degree of heterogeneity, in which multiple variables were randomly mixed at the individual neurons[6–7]. This 'random mixed selectivity' provide orthogonal neural subspaces where different neural computations can be performed independently. In light of these ideas, the moderately correlated neural subspaces between the cue and reward epochs exhibit balanced coherence and dynamics of the neural representations in the PRC, which might enable integrated processing of a targeted variable and contextual information as reported by previous studies[26–27].

In conclusion, the PRC maintained choice-direction information while representing different epochs of a task. These representations were achieved via neural dimensions shared across the cue and reward epochs despite the dynamic reorganization of the population encoding structure. The neurons with coherent responses showed their heterogeneous contribution to those dimensions, indicating reconciled coherence and dynamics of neural representations across different levels.

Methods

517

518 **Subjects**

519 Seven male Long-Evans rats (Shimizu Laboratory Supplies, Kyoto, Japan)
520 weighting 278–375 g at the beginning of the training were individually
521 housed and maintained on a laboratory light/dark cycle (lights on 8:00 A.M.
522 to 9:00 P.M.). Rats were placed on water restriction with *ad libitum* access to
523 food. The animals were maintained at 80% of their baseline weight
524 throughout the experiments. All experiments were implemented in
525 accordance with the guidelines for the care and use of laboratory animals
526 provided by the Animal Research Committee of the Doshisha University.

527

528 **Behavioral apparatus**

529 The behavioral apparatus (**Fig. 1a**) has been previously described[13,65]. An
530 operant chamber (O'Hara, Tokyo, Japan) with three ports in the front wall
531 for nose-poke responses was enclosed in a soundproof box (Brain Science
532 Idea, Osaka, Japan). Each port was equipped with an infrared sensor to
533 detect the animals' nose-poke responses. Visual cues were presented using
534 white light-emitting diodes (LEDs) (4000 mcd; RS Components, Yokohama,

535 Japan) placed on the left and right walls of the operant chamber, as in **Fig.**
536 **1a**. Cue odors were presented via the central port through a stainless tube.
537 The odors were mixed with pure air to produce a 1:10 dilution at a flow rate
538 of 60 ml/min using a custom-built olfactometer (AALBORG, Orangeburg,
539 NY). Water rewards were delivered from gravity-fed reservoirs regulated by
540 solenoid valves (The Lee Company, Westbrook, CT) through stainless tubes
541 placed inside of the left and right target-ports. We controlled stimulus and
542 reward deliveries and measured behavioral responses using Bpod and Pulse
543 Pal[66] (Sanworks, Stony Brook, NY).
544

545 **Two-alternative forced-choice task**

546 Each trial started when the rats poked their snout into the central port (**Fig.**
547 **1b**). After a variable delay (200–600ms, uniform distribution), a cue
548 randomly selected from four stimuli (left/right LED for visual modality,
549 S(+)/R(−)-2-octanol for olfactory modality) was delivered. If the rats
550 successfully maintained their nose in the central port during 1 s after the
551 cue onset, the "go" sound was delivered, and they were allowed to withdraw
552 from the central port and to choose either left or right target port based on

553 the task rule (bottom right in **Fig. 1a**). The presentations of the cue and the
554 go sound were terminated by the withdrawal from the central port. When
555 the rats left the central port without waiting for the go sound, the trial was
556 canceled and followed by a 5 s punish intertrial-interval. Only correct
557 choices were immediately rewarded by a drop of water (13 μl for five rats
558 and 16 μl for two rats), from the target port. Rats performed 861 ± 232 trials
559 in a daily recording session (seven rats, 50 sessions).

560 For two of seven rats (**Supplementary Fig. 2**), a 500 ms delay period was
561 inserted between the onset of the target choice and the reward to assess the
562 potential influence of non-orienting movements (licking) and spatial view on
563 neural responses.

564

565 **Training**

566 We trained the rats step-by-step to perform the task described above. The
567 training period typically lasted 4 to 8 weeks. First, rats were trained to
568 poke into the central port and then collect the water reward (20 μl) from the
569 left or right target-port. We gradually extended the duration of the central
570 poke by delaying the go sound up to 1 s after the poke onset. Next, the rats

571 were trained to discriminate the odor cues based on the same contingencies
572 as the recording sessions. A variable delay (200–600 ms) was inserted before
573 the cue onset. After the rats became able to successfully discriminate the
574 odor cues (> 80%), they were also trained to discriminate the visual cues
575 based on the same contingencies as the recording sessions (> 80%). Finally,
576 we interleaved visual and olfactory trials within a session and trained the
577 animals to perform the task according to a training performance criterion (>
578 80%).

579 For the two rats (**Supplementary Fig. 2**), a reward delay period was
580 introduced after they acquired the odor discrimination. The reward delay
581 was gradually extended from 100 to 500 ms.

582

583 **Mixture of odors**

584 The cue odors, S(+)/R(–)-2-octanol, were mixed together in a subset of
585 sessions in order to increase the difficulty of the olfactory discrimination
586 and thereby obtaining a sufficient number of erroneous trials. For instance,
587 we used a 60/40 ratio in a given session, delivering an odor mixture of 60%
588 S(+)-2-octanol and 40% R(–)-2-octanol. We maintained the odor

589 discrimination accuracy constant (> 80%) throughout the recording sessions

590 by adjusting the degree of odor mixing before each session.

591

592 **Surgery**

593 Rats were anesthetized with 2.5% isoflurane before surgery, and it was

594 maintained throughout surgical procedures. We monitored body

595 temperature, movements and hind leg reflex and adjusted the depth of the

596 anesthesia as needed. An eye ointment was used to keep the eyes moistened

597 throughout the surgery. Subcutaneous scalp injection of a lidocaine 1%

598 solution provided local anesthesia before the incision. The left temporalis

599 muscle was retracted to expose the skull during the surgery. A craniotomy

600 was performed over the anterior part of the left PRC (AP −3.5 to −3.24 mm,

601 ML 6.6 to 6.8 mm relative to the bregma, 3.5 to 4.0 mm below the brain

602 surface) and a custom-designed electrode was vertically implanted using a

603 stereotactic manipulator. A stainless-steel screw was placed over the

604 cerebellum and served as the ground during the recordings. We used the

605 mean response of the all electrodes as a reference. During a week of

606 postsurgical recovery, we gradually lowered the tetrodes to detect unit

607 activities in the PRC. Electrode placement was estimated based on the

608 depth and was histologically confirmed at the end of the experiments.

609

610 **Histology**

611 Once the experiments were completed, the rats were deeply anesthetized

612 with sodium pentobarbital and then transcardially perfused with

613 phosphate-buffered saline and 4% paraformaldehyde. The brains were

614 removed and post-fixed in 4% paraformaldehyde, and 100 μm coronal

615 sections of the brains were prepared to confirm the recording sites.

616

617 **Electrophysiological recordings**

618 A custom-designed electrode composed of eight tetrodes (tungsten wire, 12.5

619 μm, California Fine Wire, Grover Beach, CA) was used for the extracellular

620 recordings. The tetrodes were individually covered by a polyimide tube (A-M

621 Systems, Sequim, WA), were placed at a 100 μm separation and typically

622 had an impedance of 150–700 kΩ at 1 kHz. The signals were recorded with

623 Open Ephys (Cambridge, MA) at a sampling rate of 30 kHz and bandpass

624 filtered between 0.6 and 6 kHz. The tetrodes were lowered approximately 80

625 μm after each recording session, and thereby independent populations of

626 neurons were recorded across the sessions.

627

628 **Monitoring and processing of body posture during task performance**

629 We used a head-mounted accelerometer (Intan Technologies, Los Angeles,

630 CA) to obtain postural signals from the animals ($n = 2$) during the

631 electrophysiological recordings (**Supplementary Fig. 2**). The accelerometer

632 signals (x-, y-, z-axis) were recorded at a sampling rate of 30 kHz and then

633 downsampled to 100Hz. To precisely detect the body posture of the animals,

634 gravity components of the accelerometer signals were estimated by using a

635 low-pass filter with a cut-off frequency of 2 Hz[40]. To reduce the influence

636 from the head angle that each animal typically preferred[40], for each axis, the

637 above processed signals were normalized to the mean and standard

638 deviation in the baseline epoch (−400 to 0 ms before the cue onset).

639

640 **Spike sorting and screening criteria of units**

641 All analyses were performed using MATLAB (MathWorks, Natick, MA). To

642 detect single-neuron responses, the spikes were manually clustered with

643 MClust (A.D. Redish) for MATLAB. Only neurons met the following criteria
644 were included for further analyses: (1) units with sufficient isolation quality
645 (isolation distance ≧ 15); (2) units with reliable refractory periods
646 (violations were less than 1% of all spikes); and (3) units with sufficient
647 mean firing rates in the 1 s after the cue onset (> 0.5 Hz). On average, we
648 detected 10.9±7.4 neurons in a single recording session, and 6.2±3.4
649 neurons survived these quality criteria (total 312 neurons from seven rats).
650

651 **Selective responses to choice directions**

652 In order to evaluate the selective responses to different direction of choices,
653 we computed a choice-direction selectivity[67]. We first grouped correct trials
654 into four types based on the cue modality (visual or olfactory) and target
655 choice (left or right). For each modality, we independently calculated the
656 choice-direction selectivity by using ROC analysis[68]. The choice-direction
657 selectivity was obtained from the area under ROC curve (AUC) and defined
658 as 2 × (AUC−0.5) ranging from −1 to 1. In our analysis, a positive value
659 indicated a neuron selectively fired to the left target-choice, and a negative
660 value indicated the opposite. A value of zero indicated the absence of choice-

direction selective responses. To determine statistical significance ($P < 0.05$), we used permutation tests (1,000 interactions). For visualization of the temporal patterns of the choice-direction selectivity in individual neurons (**Fig. 2a, Fig.3, Supplementary Fig. 1, and Supplementary Fig. 2b**), mean firing rates were computed in 10 ms time windows (smoothed with a Gaussian, σ = 30 ms), and we then computed the choice-direction selectivity at each time point from those data.

Statistics

We evaluated the statistical significance of the decoding analysis and the state space analysis with a bootstrapping procedure[8]. We estimated the P value for the bootstrapping procedure by computing the ratio $(1+X) / (N+1)$, where the number X indicates overlapping data points between the two distributions and the number N indicates interactions. Since we used 1,000 bootstraps, two distributions with no overlap resulted in $P < 0.001$, and two distributions with x% overlap resulted in $P \approx x/100$.

All the data are presented as mean ± standard deviation, unless otherwise stated.

679

680 **Decoding analysis**

681 We employed a cross-temporal pattern analysis[42, 59, 69] to investigate the
682 temporal changes in the choice-direction selective responses in the PRC.
683 Neural responses were pooled across the recording sessions to maximize the
684 number of neural responses included in the decoding analysis. Here, we
685 refer to the pooled pseudo-population of the PRC neurons (n = 207 from five
686 rats) as the full population. The instantaneous firing rate of each neuron
687 was estimated by the spike counts in a 150 ms sliding window (10 ms
688 increment). We computed the above described choice-direction selectivity
689 from the instantaneous firing rates for each neuron independently for visual
690 and olfactory trials. In this manner, we generated two independent
691 population vectors for the full population (cells × time matrix each for the
692 cue modalities). We obtained a pattern similarity index by calculating the
693 Fisher-transformed Pearson correlation (r) between these two population
694 vectors. This index provided the pattern similarity for both equivalent and
695 different time points (for example, **Fig. 4a**). A positive value was interpreted
696 as evidence for a reliable choice-direction encoding irrespective of the cue

modality.

To estimate the mean performance values for the pattern classification analysis, we randomly resampled the neurons (the same number of neurons as neural population analyzed) and computed the choice-direction selectivity in visual and olfactory trials. Neural responses were aligned to withdrawal onset from the central port (for a cue epoch), target-choice onset (for a reward epoch) and target-choice offset (for two return-epochs). For return-epoch responses, we analyzed neural responses before and after the animals left the target ports in preparation for the next trials (pre-return epoch: −400 to 0 ms before leaving a target port: post-return epoch: 0 to 400 ms after leaving a target port). Only trials where the animals directly returned from the target port to the central port for the next trial were included in the analysis. These data allowed us to compute the pattern similarity indices within an epoch or across two different epochs. To investigate choice-direction encoding during the epochs, we averaged the performance within each of the epochs (the cue, reward, pre-return and post-return epochs). To obtain a baseline performance, we averaged the classification performance during the baseline epoch, −400 to 0 ms before the cue onset. We also

quantified the pattern similarity of the neural responses between two epochs (for simplicity, we here refer to these epochs as A-epoch and B-epoch) by averaging the following two pattern classifications: pattern classification for A-epoch responses in visual trials and B-epoch responses in olfactory trials, and A-epoch responses in olfactory trials and B-epoch responses in visual trials (for example, **Fig. 4c**). We repeated the above processes 1,000 times to obtain a distribution of 1,000 different measurements of each pattern classification. To determine statistical significance, we compared a distribution obtained from 1,000 different pattern classification measurements within an epoch with a baseline distribution using the above described estimated P value. We considered zero to be chance level instead of the baseline distribution when we verified statistical significance of the classification across the epochs.

Decoding analysis of erroneous trials

We included 119 neurons recorded in sessions with a sufficient number of erroneous target-choices (at least 11 trials for both directions of target-choice) in all the analyses for erroneous trials. Due to the similarity of the

choice-direction selectivity between the different cue-modalities in correct trials (**Fig. 2c** and **4a**), we computed the pattern similarity index using correct visual trials and erroneous olfactory trials to evaluate the influence of erroneous behavioral performance on the choice-direction encoding (**Fig. 4e**). In the erroneous trials, the animals chose the same target-port as the correct trials. To determine statistical significance of pattern classification performance in correct and erroneous trials, we downsampled the correct olfactory trials to match the number of trials for the erroneous olfactory trials (**Fig. 4f**). To test whether the classification performance during each epoch decreased from the correct trials to erroneous trials, we subtracted the classification performance in the erroneous trials from that in the correct trials for each resampling. The distribution of the residual performance was compared with zero by using the estimated P value.

State space analysis

To understand the population structure and its temporal change between the cue and reward epochs, we performed principal component analysis (PCA). For each of the epochs, we constructed a 207 neurons × 4 conditions

751 matrix[43–44], in which columns contained trial-averaged z-scored firing rates
752 of each neuron. The instantaneous firing rate of each neuron (estimated by
753 spike counts in a 150 ms sliding window with 10 ms increment) was
754 converted to a z-score by normalizing to the mean and standard deviation of
755 its own instantaneous firing rates during the epoch. We then obtained time-
756 averaged firing rates of the neurons each for the cue and reward epochs.
757 By performing PCA on these datasets, we reduced the dimensionality of the
758 PRC population from 207 neurons to two principal components
759 (**Supplementary Fig. 5a**). We independently performed this analysis for
760 population responses during the cue and reward epochs to obtain the cue-
761 epoch and reward-epoch subspaces.
762 For data projections onto the above two-dimensional neural subspaces, we
763 randomly selected 25 trials for each of the four conditions. z-scored firing
764 rates of each neuron were then obtained by normalizing the data to the
765 mean and standard deviation of its own firing rates during the epoch
766 corresponding to the neural subspaces in which the projections were
767 performed. We averaged the z-scored firing rates of each neuron during each
768 of three epochs (the cue, reward and baseline epochs) to obtain a 207 cells ×

4 conditions matrix for each epoch. To visualize the population responses, we projected these data onto the two-dimensional PCA space. This allowed us to obtain a single point reflecting the entire population response for each of the four conditions. We repeated this procedure five times with different subsets of 25 trials, and this allowed us to reduce some degree of the variability among individual trials. To obtain the within-condition distance, we computed the mean of pairwise Euclidean distances for five points in each of the four conditions and then averaged those distances across the conditions to obtain a single value for the within-condition distance. To obtain the across-condition distance, we computed pairwise distances between two sets of five points obtained from two different conditions in the same subspace and then averaged them. This procedure was repeated for all possible combinations of two different conditions, and we then averaged those distances to obtain a single value for the across-condition distance. We also investigated how the representational geometry changed between different epochs (that is, temporal shift of population responses in a neural subspace). This was achieved by computing the mean of pairwise distances between two sets of five points obtained from neural responses under a

single condition in two different epochs. The mean distance was obtained for all trial conditions and then averaged to produce a single value for the across-condition distance for the temporal shifts.

To visualize variability across different subsets of trials (**Fig. 5a**) and test statistical significance, the above analysis was repeated 1,000 times with different subsets of resampled trials. The across-condition distances of the projections on corresponding subspaces (that is, cue-epoch responses onto cue-epoch subspace and reward-epoch responses onto reward-epoch subspace; **Fig.5a**) were compared with a distribution of the within-condition distance using the above described estimated P value (**Fig. 5b**). Across-condition distances larger than within-condition distance indicated that different trial conditions were discriminated at the population level. Similarly, the across-condition distances of projections onto the interchanged subspaces (that is, cue-epoch responses onto reward-epoch subspace and reward-epoch responses onto cue-epoch subspace; **Fig. 5a**) were compared with a distribution of within-condition distance by using the estimated P value (**Fig. 5c**). For the projections onto the interchanged subspaces, we also projected baseline-epoch responses as negative controls

805 (**Fig. 5c and Supplementary Fig. 5c**). To investigate the importance of the
806 temporal response patterns of individual neurons, we projected randomly
807 shuffled data (**Fig. 5c and g**), where the correspondence between the cue-
808 epoch responses and reward-epoch responses were shuffled among the
809 neurons (**Supplementary Fig. 5d**). We considered across-condition distances
810 of the baseline-epoch responses to be chance when we evaluated the
811 temporal shifts in representational geometry between the cue and reward
812 epoch in a neural subspace (**Fig. 5g**).
813 To directly evaluate contribution of individual neurons to the choice-
814 direction encodings (**Fig. 5f**), we performed the following analysis. We first
815 sorted all the neurons from ones with the highest magnitude of the
816 weighting values on the first dimension of the cue or reward epoch. For
817 these differently sorted populations, we performed cluster projections onto
818 the corresponding subspaces with increasing numbers of neurons. For
819 precise evaluation of each neuron's contribution, rather than performing
820 PCA on each of differently sized populations independently, we used the
821 same projection data in **Fig. 5a** (that is, the full population data) and
822 replaced the weighting values of excluded neurons with zero. In each size of

population, across-condition distance for different choice-directions on the first dimension was computed for each modality and then averaged. Those distances were then normalized to the distance obtained from the full population. We compared the distances from differently sized populations with those from the full population by the estimated P value. When the estimated P exceeded 0.05, we considered that number of neurons was sufficient to achieve discriminability of the choice directions equivalent to the full population.

Relationship between choice-direction and task-epoch discriminability

To understand how the PRC neural population reconciled coherent representations of the choice directions (**Fig. 5c**) with dynamic changes for different task-epochs (**Fig. 5g**), we performed the following analyses. First, to quantify the degree of representational coherence in the PRC neural responses between the cue and reward epochs, the 1,000 across-condition distances of interchanged projections (for example, the reward-epoch responses onto the cue-epoch subspace shown in **Fig. 5c**) were divided by the 1,000 across-condition distances of the corresponding projections (for

841 example, the cue-epoch responses onto the cue-epoch subspace shown in **Fig.**
842 **5b**). We repeated this procedure for projections of each of the cue and reward
843 subspaces and then averaged between them to obtain the 1,000 normalized
844 distances. Those normalized distances reflected the degree of
845 discriminability of the different trial conditions preserved across the
846 different epochs, and we referred those values as a temporal coherence
847 index (x-axis in **Fig. 5h**). As negative controls, for each of the cue and reward
848 subspace, the across-condition distances from the interchanged projections
849 of the baseline-epoch responses and the randomly shuffled responses (**Fig.**
850 **5c**) were also divided by the across-condition distances of the corresponding
851 projections (**Fig. 5b**), and we then averaged them between the epochs (**Fig.**
852 **5h**). Second, to quantify the degree of dynamic changes in the PRC neural
853 responses between the cue and reward epochs, the 1,000 cluster distances
854 obtained from temporal shifts of the population responses in a neural
855 subspace (for example, distances from the cue-epoch responses to the
856 reward-epoch responses in the cue-epoch subspace, which was computed for
857 **Fig. 5g**) were divided by the 1,000 cluster distances obtained from simulated
858 maximum temporal shifts of population responses in the same neural

subspace (in this case, distances from the cue-epoch responses to the completely inverted cue-epoch responses in the cue-epoch subspace). The simulated neural responses were produced by inverting signs of the original projection data in the first and second dimensions. We repeated this procedure for projection data on each of the cue and reward subspaces and then averaged between them to obtain the 1,000 normalized distances. Those normalized distances reflected the degree of discriminability of the different epochs (that is, the cue and reward epochs), we therefore referred those values as a temporal shift index (y-axis in **Fig. 5h**). Given the procedures for identifying neural subspaces by PCA, in which the neural responses were mean-centered in each epoch, we did not suppose any types of representational geometry that were not centralized or had temporal changes with deviation from the range of across-condition distances in the corresponding projections. Therefore, the completely inverted response pattens provided the maximum level of temporal shifts (temporal shift index = 1). This also indicates that the temporal shift index equals 0.5 when projected clusters overlap on the center of neural subspaces. As negative controls, for each of the cue and reward subspace, the temporal shift

distances from the interchanged projections of the baseline-epoch responses and randomly shuffled responses (**Fig. 5g**) were also divided by the cluster distances obtained from the above described simulated temporal shifts of population responses and then averaged between the epochs.

Data availability

The data sets analyzed in the present study are available from the corresponding authors upon reasonable request.

Code availability

The code used for analysis in the present study are available from the corresponding authors upon reasonable request.

References

1. Sakurai,Y. et al. Multipotentiality of the brain to be revisited repeatedly. *The Physics*

of the Mind and Brain Disorders: pp.513–525. (Springer, Cham, 2017)

2. Sakurai, Y. Cells in the rat auditory system have sensory-delay correlates during the performance of an auditory working memory task. *Behav. Neurosci.* **104**, 856–868 (1990).

3. Sakurai, Y. Hippocampal cells have behavioral correlates during the performance of an auditory working memory task in the rat. *Behav. Neurosci.* **104**, 253–263 (1990).

4. Elsayed, G. F., Lara, A. H., Kaufman, M. T., Churchland, M. M. & Cunningham, J. P. Reorganization between preparatory and movement population responses in motor cortex. *Nat. Commun.* **7**, 13239 (2016).

5. Lara, A. H., Cunningham, J. P. & Churchland, M. M. Different population dynamics in the supplementary motor area and motor cortex during reaching. *Nat. Commun.* **9**, (2018).

6. Mante, V., Sussillo, D., Shenoy, K. V & Newsome, W. T. Context-dependent

computation by recurrent dynamics in prefrontal cortex. *Nature*. **503**, 78–84 (2013).

7. Raposo, D., Kaufman, M. T. & Churchland, A. K. A category-free neural population supports evolving demands during decision-making. *Nat. Neurosci.* **17**, 1784–1792 (2014).

8. Parthasarathy, A. et al. Mixed selectivity morphs population codes in prefrontal cortex. *Nat. Neurosci.* **20**, 1770–1779 (2017).

9. Mendoza-Halliday, D. & Martinez-Trujillo, J. C. Neuronal population coding of perceived and memorized visual features in the lateral prefrontal cortex. *Nat. Commun.* **8**, 15471 (2017).

10. Kennerley, S. W. & Wallis, J. D. Evaluating choices by single neurons in the frontal lobe: outcome value encoded across multiple decision variables. *Eur. J. Neurosci.* **29**, 2061–2073 (2009).

11. Gardner, M. P. H. & Fontanini, A. Encoding and tracking of outcome-specific

931 expectancy in the gustatory cortex of alert rats. *J. Neurosci.* **34**, 13000–13017
932 (2014).
933
934 12. Guo, Z. V. et al. Maintenance of persistent activity in a frontal thalamocortical loop.
935 *Nature*. **545**, 181–186 (2017).
936
937 13. Hirokawa, J., Vaughan, A., Masset, P., Ott, T. & Kepecs, A. Frontal cortex neuron
938 types categorically encode single decision variables. *Nature* **576**, 446–451 (2019).
939
940 14. Furuyashiki, T., Holland, P. C. & Gallagher, M. Rat orbitofrontal cortex separately
941 encodes response and outcome information during performance of goal-directed
942 behavior. *J. Neurosci.* **28**, 5127–5138 (2008).
943
944 15. Hosokawa, T., Kato, K., Inoue, M. & Mikami, A. Correspondence of cue activity to
945 reward activity in the macaque orbitofrontal cortex. *Neurosci. Lett.* **389**, 146–151
946 (2005).
947
948 16. Eradath, M. K., Mogami, T., Wang, G. & Tanaka, K. Time context of cue-outcome

associations represented by neurons in perirhinal cortex. *J. Neurosci.* **35**, 4350–4365 (2015).

17. Ahn, J.R. & Lee, I. Neural correlates of both perception and memory for objects in the rodent perirhinal cortex. *Cereb. Cortex.* **27**, 3856–3868 (2017).

18. Ahn, J.R. & Lee, I. Neural correlates of object-associated choice behavior in the perirhinal cortex of rats. *J. Neurosci.* **35**, 1692–1705 (2015).

19. Naya, Y., Yoshida, M. & Miyashita, Y. Forward processing of long-term associative memory in monkey inferotemporal cortex. *J. Neurosci.* **23**, 2861–2871 (2003).

20. Naya, Y., Yoshida, M., Takeda, M., Fujimichi, R. & Miyashita, Y. Delay-period activities in two subdivisions of monkey inferotemporal cortex during pair association memory task. *Eur. J. Neurosci.* **18**, 2915–2918 (2003).

21. Naya, Y., Sakai, K. & Miyashita, Y. Activity of primate inferotemporal neurons related to a sought target in pair-association task. *Proc. Natl. Acad. Sci. U. S. A.* **93**,

2664–2669 (1996).

22. Sakai, K. & Miyashita, Y. Neural organization for the long-term memory of paired associates. *Nature*. **354**, 152–155 (1991).

23. Burwell, R. D. Borders and cytoarchitecture of the perirhinal and postrhinal cortices in the rat. *J. Comp. Neurol.* **437**, 17–41 (2001).

24. Furtak, S. C., Wei, S.M., Agster, K. L. & Burwell, R. D. Functional neuroanatomy of the parahippocampal region in the rat: the perirhinal and postrhinal cortices. *Hippocampus* **17**, 709–722 (2007).

25. Tomas Pereira, I. et al. Subcortical connections of the perirhinal, postrhinal, and entorhinal cortices of the rat. I. afferents. *Hippocampus* **26**, 1189–1212 (2016).

26. Naya, Y., Chen, H., Yang, C. & Suzuki, W. A. Contributions of primate prefrontal cortex and medial temporal lobe to temporal-order memory. *Proc. Natl. Acad. Sci. U. S. A.* **114**, 13555–13560 (2017).

27. Naya, Y. & Suzuki, W. A. Integrating what and when across the primate medial temporal lobe. *Science*. **333**, 773–776 (2011).

28. Shiotani, K. et al. Tuning of ventral tenia tecta neurons of the olfactory cortex to distinct scenes of feeding behavior. Preprint at https://www.biorxiv.org/content/10.1101/455089v1 (2018).

29. Harvey, C. D., Coen, P. & Tank, D. W. Choice-specific sequences in parietal cortex during a virtual-navigation decision task. *Nature* 484, 62–68 (2012).

30. Akhlaghpour, H. et al. Dissociated sequential activity and stimulus encoding in the dorsomedial striatum during spatial working memory. *Elife* **5**, e19507 (2016).

31. Hwang, E. J., Dahlen, J. E., Mukundan, M. & Komiyama, T. History-based action selection bias in posterior parietal cortex. *Nat. Commun*. **8**, 1242 (2017).

32. Fujisawa, S., Amarasingham, A., Harrison, M. T. & Buzsáki, G. Behavior-dependent

short-term assembly dynamics in the medial prefrontal cortex. *Nat. Neurosci.* **11**, 823 (2008).

33. Handa, T., Takekawa, T., Harukuni, R., Isomura, Y. & Fukai, T. Medial frontal circuit dynamics represents probabilistic choices for unfamiliar sensory experience. *Cereb. Cortex* **27**, 3818–3831 (2017).

34. Siniscalchi, M. J., Wang, H. & Kwan, A.C. Enhanced population coding for rewarded choices in the medial frontal cortex of the mouse. *Cereb. Cortex*, **29**, 4090–4106 (2019).

35. Musall, S., Kaufman, M.T., Juavinett, A.L., Gluf, S. & Churchland, A.K. Single-trial neural dynamics are dominated by richly varied movements. *Nat. Neurosci.* **22**, 1677–1686 (2019).

36. Krumin, M., Lee, J.J., Harris, K.D., & Carandini, M. Decision and navigation in mouse parietal cortex. *eLife* **7**, e42583 (2018).

37. Wang, C. et al. Egocentric coding of external items in the lateral entorhinal cortex. *Science* **362**, 945–949 (2018).

38. Erlich, J. C., Bialek, M. & Brody, C. D. A cortical substrate for memory-guided orienting in the rat. *Neuron* **72**, 330–343 (2011).

39. Steinmetz, N.A., Zatka-Haas, P., Carandini, M. & Harris, K.D. Distributed coding of choice, action and engagement across the mouse brain. *Nature* **576,** 266–273 (2019).

40. Meyer, A.F., Poort, J., O'Keefe, J., Sahani, M. & Linden, J.F. A Head-mounted camera system integrates detailed behavioral monitoring with multichannel electrophysiology in freely moving mice. *Neuron* **100**, 46–60 (2018).

41. Yoshizawa, T., Ito, M. & Doya, K. Reward-predictive neural activities in striatal striosome compartments. *eNeuro*, **5**, e0367-17. (2018).

42. Stokes, M. G. et al. Dynamic coding for cognitive control in prefrontal cortex.

Neuron. **78**, 364–375 (2013).

43. Cavanagh, S. E., Towers, J. P., Wallis, J. D., Hunt, L. T. & Kennerley, S. W. Reconciling persistent and dynamic hypotheses of working memory coding in prefrontal cortex. *Nat. Commun*. **9**, 1–16 (2018).

44. Murray, J. D. et al. Stable population coding for working memory coexists with heterogeneous neural dynamics in prefrontal cortex. *Proc. Natl Acad. Sci*. USA **114**, 394–399 (2017).

45. Morcos, A. & Harvey, C. History-dependent variability in population dynamics during evidence accumulation in cortex. *Nat Neurosci* **19,** 1672–1681 (2016).

46. Mendoza-Halliday, D., Martinez-Trujillo, J. Neuronal population coding of perceived and memorized visual features in the lateral prefrontal cortex. *Nat Commun.* **8,** 15471 (2017).

47. Liu, Z., Murray, E. A. & Richmond, B. J. Learning motivational significance of

visual cues for reward schedules requires rhinal cortex. *Nat. Neurosci.* **3**, 1307–1315 (2000).

48. Clark, A. M., Bouret, S., Young, A. M. & Richmond B. J. Intersection of reward and memory in monkey rhinal cortex. *J. Neurosci.* **32**, 6869–6877 (2012).

49. Mogami, T. & Tanaka, K. Reward association affects neuronal responses to visual stimuli in macaque TE and perirhinal cortices. *J. Neurosci.* **26**, 6761–6770 (2006).

50. Ohyama, K., Sugase-Miyamoto, Y., Matsumoto, N., Shidara, M. & Sato, C. Stimulus-related activity during conditional associations in monkey perirhinal cortex neurons depends on upcoming reward outcome. *J. Neurosci.* **32**, 17407–17419 (2012).

51. Ahn, J.R., Lee, H.W. & Lee, I. Rhythmic Pruning of Perceptual Noise for Object Representation in the Hippocampus and Perirhinal Cortex in Rats. *Cell Rep.* **26**, 2362–2376 (2019).

52. Bartko, S. J., Winters, B. D., Cowell, R. A., Saksida, L. M. & Bussey, T. J. Perceptual functions of perirhinal cortex in rats: zero-delay object recognition and simultaneous oddity discriminations. *J Neurosci* **27**, 2548–2559 (2007).

53. Nelson, A.J., Olarte-Sánchez, C.M., Amin, E. & Aggleton, J.P. Perirhinal cortex lesions that impair object recognition memory spare landmark discriminations. *Behav. Brain Res.* **313**, 255–259 (2016).

54. Ho, J. W. et al. Bidirectional modulation of recognition memory. *J. Neurosci.* **35**, 13323–13335 (2015).

55. Kreher, M.A. et al. The perirhinal cortex supports spatial intertemporal choice stability. *Neurobiol. Learn. Mem.* **162**, 36–46 (2019).

56. Bos, J.J. et al. Perirhinal firing patterns are sustained across large spatial segments of the task environment. *Nat. Commun.* **8**, 15602 (2017).

57. Meunier, M., Bachevalier, J., Mishkin, M. & Murray, E. A. Effects on visual

recognition of combined and separate ablations of the entorhinal and perirhinal cortex in rhesus monkeys. *J. Neurosci.* **13**, 5418–5432 (1993).

58. Jun, J. K. et al. Heterogenous population coding of a short-term memory and decision task. *J. Neurosci.* **30**, 916–929 (2010).

59. Spaak, E., Watanabe, K., Funahashi, S. & Stokes, M. G. Stable and Dynamic Coding for Working Memory in Primate Prefrontal Cortex. *J. Neurosci.* **37**, 6503–6516 (2017).

60. Meister, M. L., Hennig, J. A. & Huk, A. C. Signal multiplexing and single-neuron computations in lateral intraparietal area during decision-making. *J. Neurosci.* **33**, 2254–2267 (2013).

61. Rigotti, M. et al. The importance of mixed selectivity in complex cognitive tasks. *Nature* **497**, 585–590 (2013).

62. Barak, O., Rigotti, M. & Fusi, S. The sparseness of mixed selectivity neurons

controls the generalization-discrimination trade-off. *J. Neurosci.* **33**, 3844–3856 (2013).

63. Miller, E. K. & Fusi, S. Limber neurons for a nimble mind. *Neuron* **78**, 211–213 (2013)

64. Churchland, M. M. & Shenoy, K. V. Temporal complexity and heterogeneity of single-neuron activity in premotor and motor cortex. *J. Neurophysiol.* **97**, 4235–4257 (2007).

65. Osako, Y., Sakurai, Y. & Hirokawa, J. Subjective decision threshold for accurate visual detection performance in rats. *Sci. Rep.* **8**, 1–10 (2018).

66. Sanders, J. I. & Kepecs, A. A low-cost programmable pulse generator for physiology and behavior. *Front. Neuroeng.* **7**, 1–8 (2014).

67. Hirokawa, J. et al. Multisensory information facilitates reaction speed by enlarging activity difference between superior colliculus hemispheres in rats. *PLoS One* **6**,

(2011).

68. Green D. M. & Swets J. A. Signal detection theory and psychophysics. (Wiley, New York, 1966)

69. Wasmuht, D. F., Spaak, E., Buschman, T. J., Miller, E. K. & Stokes, M. G. Intrinsic neuronal dynamics predict distinct functional roles during working memory. *Nat. Commun.* **9**, (2018).

Acknowledgments

We would like to thank members of the Laboratory of Neural Information at Doshisha University for helpful discussion, and Y. Tanisumi for help with visualization of the data. This research was supported by the JSPS KAKENHI Grant Numbers 19J12634 (to T.O.), 16H02061, 18H05088 (to Y.S.) and 16K18380 (to J.H.).

Author contributions

T.O., Y.S., and J.H. designed the experiments. T.O. performed the experiments and analyzed the data. Y.O. analyzed the data. H.M, Y.S. and J.H. supervised the project. All authors contributed to writing the manuscript.

Competing interests

The authors declare no competing interests.

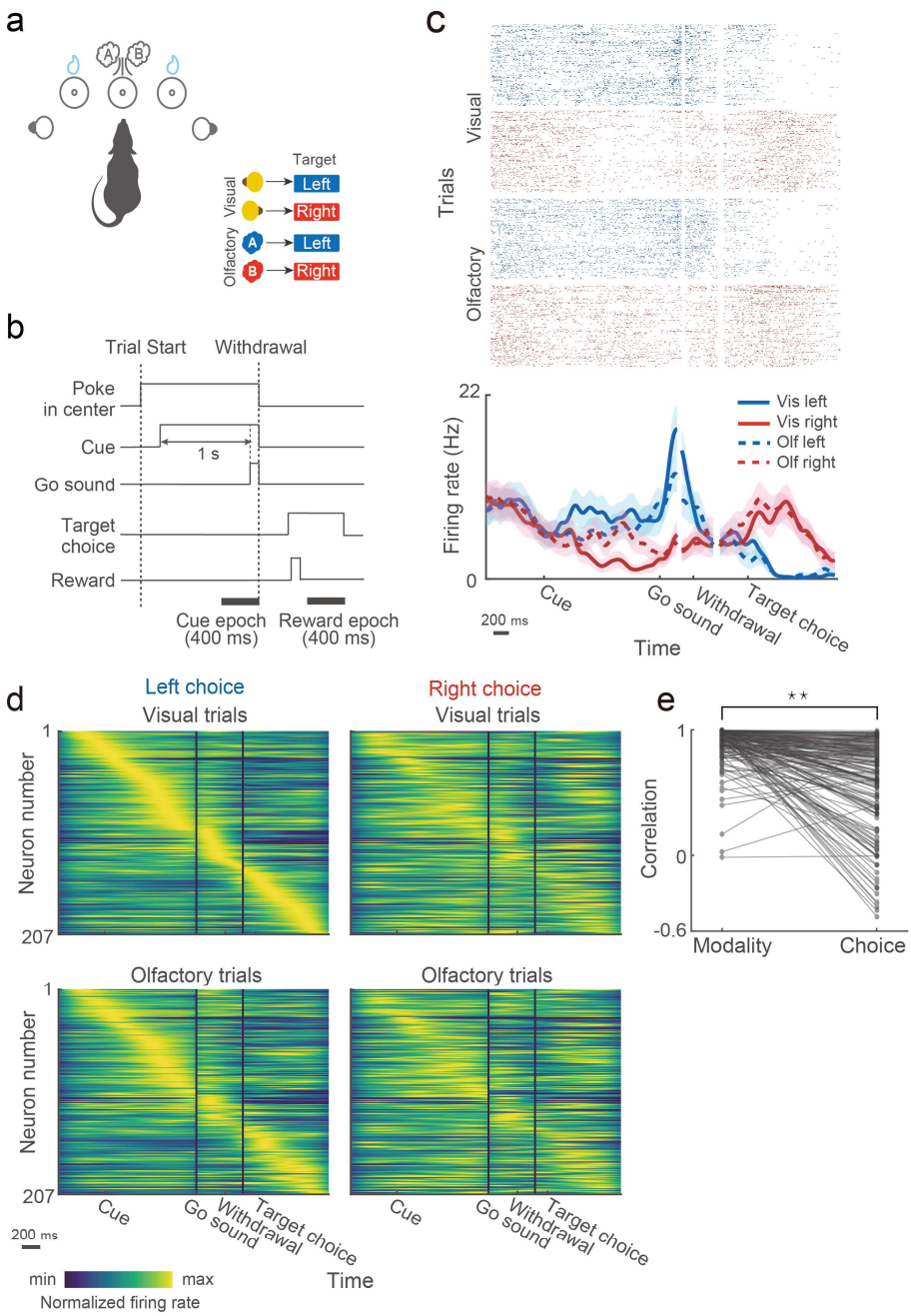

Figure 1 | Firing patterns of the PRC neurons in a two-alternative forced-choice task. (**a**) Schematic drawing of the behavioral apparatus and the cue-target associative relationships. (**b**) Schematic of the task timeline. (**c**) Raster plot and peri-event time histogram showing response of a

representative neuron. Trial types are classified according to cue modality and target choice as follows: blue, left target-choices; red, right target-choices; solid line, visual trials; dashed line; olfactory trials. Neural responses in correct trials were independently aligned to cue, withdrawal and target-choice onset and then reconstructed because of variable time between them. Lines and shaded areas indicate mean and s.e.m., respectively. (**d**) Firing patterns across all the neurons (n = 207) for the different trial conditions. In each trial type, mean firing rate of each neuron was normalized to its peak. For all trial types, the neurons were sorted by their peak firing time in visually-cued left choice trials (upper left). (**e**) Comparison of temporal firing patterns of individual neurons between the different modalities and choice directions. For comparison between different modalities, for each neuron, correlation coefficients were computed between peak-normalized firing rates in visual left (upper left in d) and olfactory left trials (bottom left in d). For comparison between different choices, correlation coefficients were computed between peak-normalized firing rates in visual left (upper left in d) and visual right trials (upper right in d). Nearly identical results were achieved when correlations were computed

1179 between the visual right and olfactory right trials and between the visual

1180 right and olfactory right trials (data not shown).

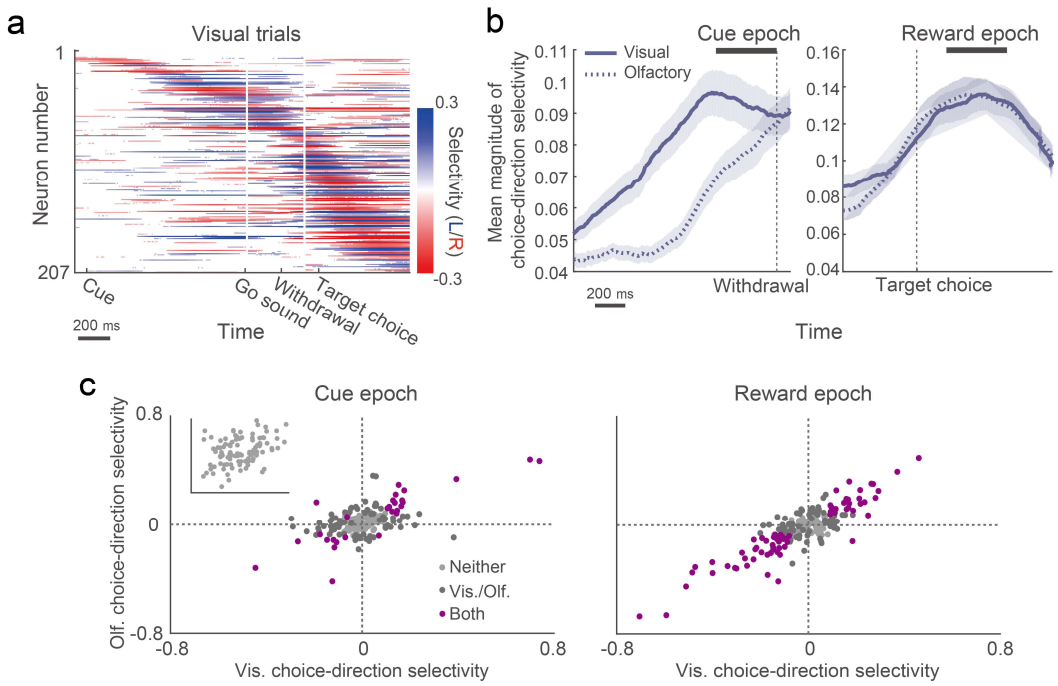

1181

1182 **Figure 2 | Choice-direction selectivity of the individual PRC neurons in**

1183 **different epochs of the task.** (**a**) Temporal patterns of choice-direction

1184 selective responses of the PRC neurons (n = 207) in correct visual trials.

1185 Colors indicate selectivity to the left (blue) or right (red) choice. Neurons

1186 were sorted according to the time of their peak selectivity. Only segments

1187 with significant selectivity are shown (P < 0.05; 1,000 permutations). (**b**)

1188 Time course of the choice-direction selectivity magnitude in visual (solid

1189 line) and olfactory (dashed line) trials averaged across all the neurons.

Neural responses around the withdrawal onset (left) and target-choice onset (right) are shown. Lines and shaded areas indicate mean and s.e.m., respectively. (**c**) Scatter plots showing the choice-direction selectivity of the neural population during the cue (left) and reward (right) epochs (n = 207 neurons). Each point corresponds to values of a single neuron. Colors indicate significance (P < 0.05; 1,000 permutations): light gray, no selectivity; deep gray, significant in either cue modality; purple significant in both cue modalities. Inset, the choice-direction selectivity of the non-selective neurons (n = 101) in the cue epoch.

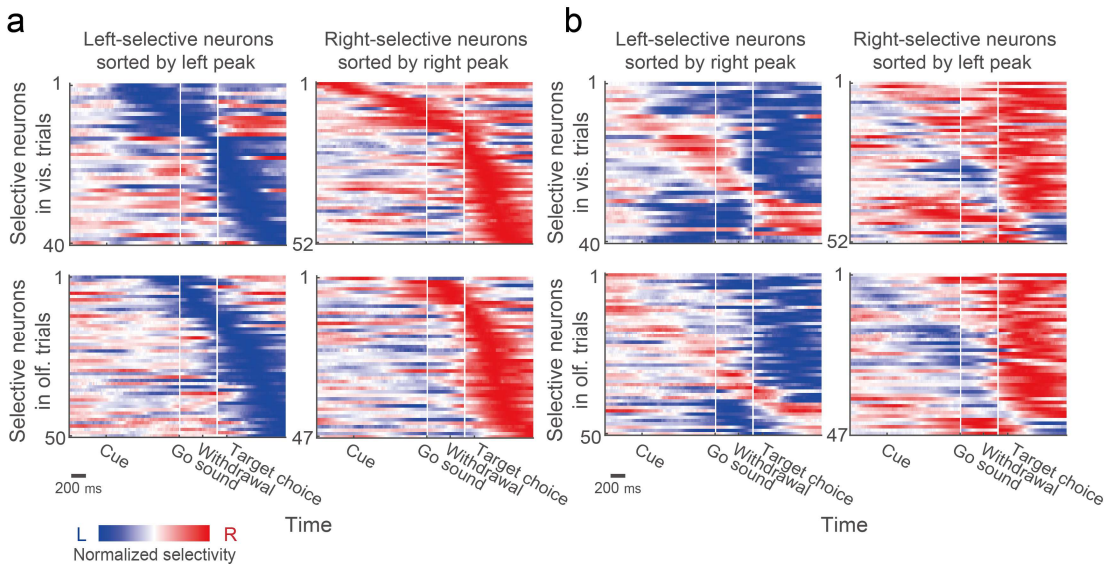

Figure 3 | Time-varying choice-direction selectivity in individual neurons. (**a**) Temporal response patterns of left-selective and right-selective subpopulations. In each modality, neurons were classified by their peaks of

significant choice-direction selectivity (Fig. 2a and Supplementary Fig.1). The selectivity of each neuron was normalized to its peak. The neurons were sorted according to the time of their peak selectivity. To visualize the entirety of time-varying selectivity, all segments with and without statistical significance are shown. (b) Same as in a, except for that the neurons were sorted by their peak selectivity to the opposite choice direction.

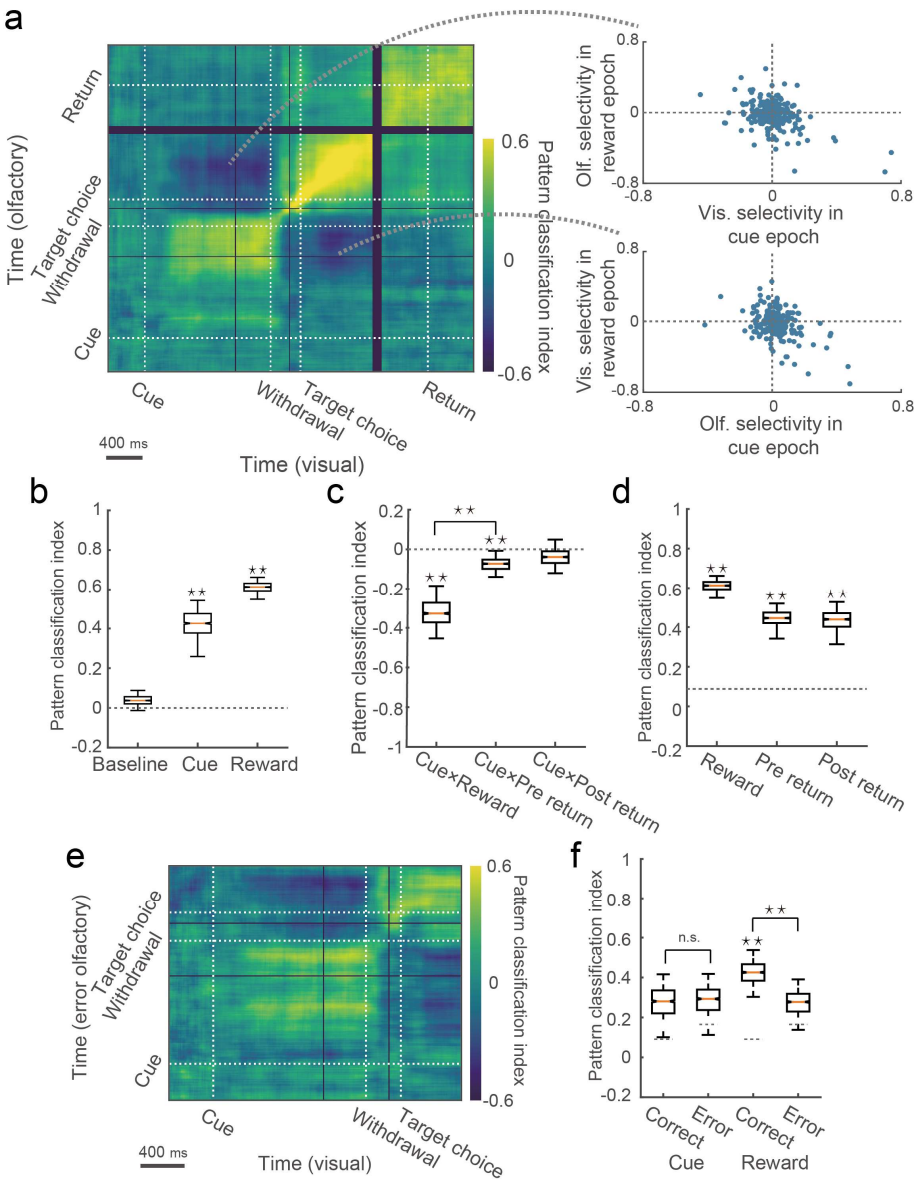

Figure 4 | Time-resolved pattern analysis for temporal changes of choice-direction selectivity. (a) Performance of the pattern classification analysis (left). White lines correspond to the onset time of cue, withdrawal, target choice, and return movement to the central port (target-choice offset). We trained a classifier using neural responses in correct visual trials to

discriminate choice directions and tested them with neural responses in correct olfactory trials (n = 207 neurons). Temporal inversions of choice-direction selectivity between the cue and reward epochs are shown by scatter plots (right). (**b**) Mean classification performance during the baseline, cue and reward epochs. (**c**) Mean classification performance across two different epochs. (**d**) Mean classification performance during the reward, pre-return and post-return epochs. Dashed line indicates the 97.5th percentile values of the baseline distribution shown in b. (**e**) A classifier tested with erroneous olfactory trials (n = 119 neurons). (**f**) Mean classification performance in erroneous trials compared with correct trials. Dashed lines indicate the 97.5th percentile values of the baseline distributions in the correct and erroneous trials. In box plots: orange line, median; box limits, 25th and 75th quartiles; notch limits, (1.57×interquartile range)/$\sqrt{n}$; whiskers, 95th percentile range (two-sided) of the distribution. Asterisks indicate statistical significance based on estimated P values ($P < 0.05$; Methods), and n.s. indicate insignificance.

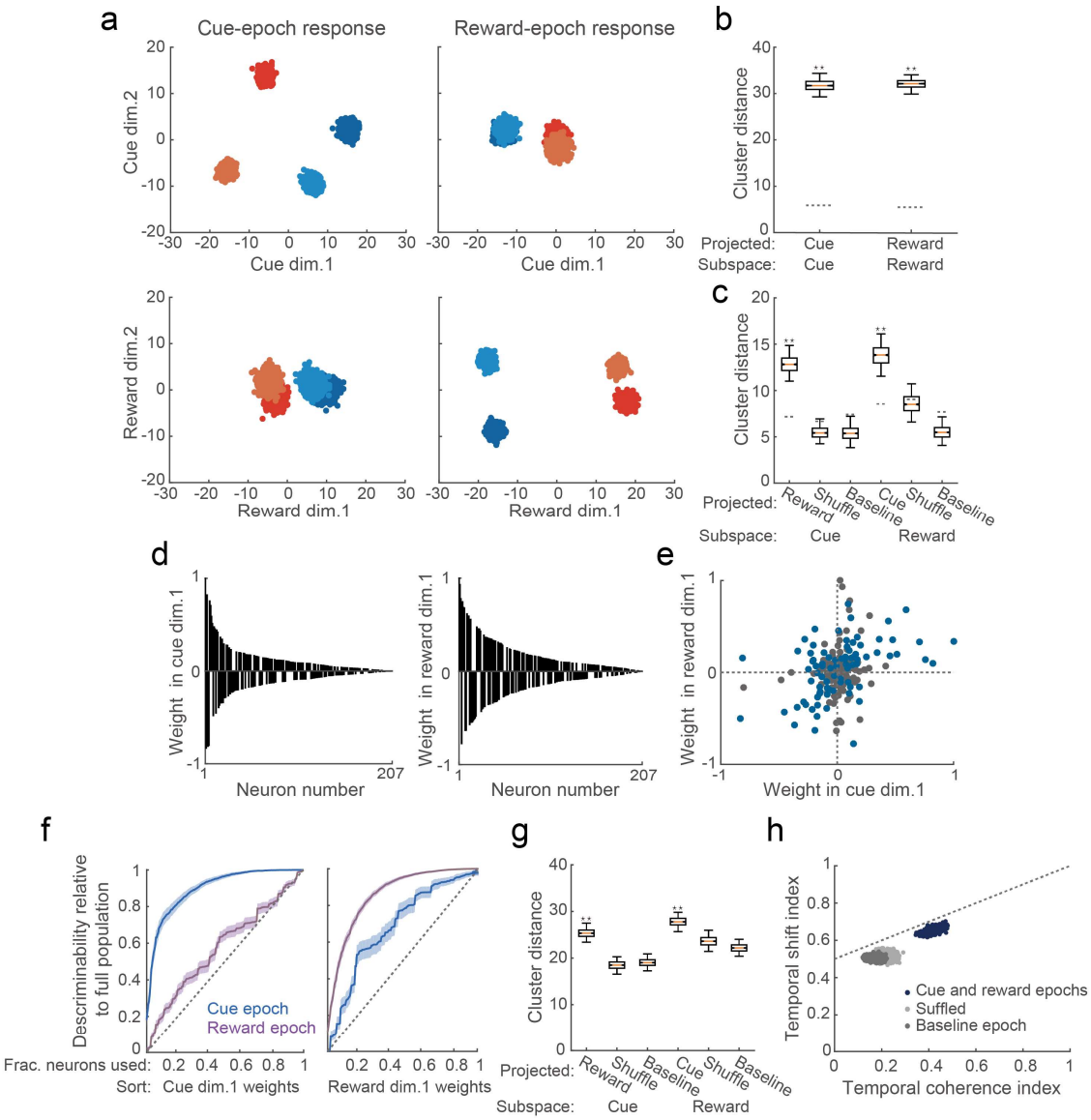

Figure 5 | Principal component analysis of neural population responses. (**a**) Population responses during cue and reward epochs projected onto the first two dimensions of cue-epoch and reward-epoch subspaces. Blue, left target-choice in visual trials; pale blue, left target-choice in olfactory trials; red, right target-choice in visual trials; orange, right target-choice in

1237 olfactory trials. Each point corresponds to the population response in a
1238 subset of trials. (**b**–**c**) Comparisons between across-condition distances and
1239 within-condition distances. Dashed lines indicate the 97.5th percentile
1240 ranges of within-condition distances.(**b**) Distances obtained from projections
1241 onto corresponding subspaces. (**c**) Distances obtained from projections onto
1242 interchanged subspaces. (**d**) Weights of individual neurons in the first
1243 dimensions of the cue-epoch (left) and reward-epoch (right) subspaces shown
1244 in a. The values were normalized by magnitude of the highest weighting
1245 value and were ordered by magnitude. (**e**) Correlation between the neural
1246 weights in the first dimensions of the cue and reward subspaces shown in d.
1247 Blue points, neurons with significant choice-direction selectivity ($P < 0.05$)
1248 across the cue and reward epochs. (**f**) Choice-direction discriminability by
1249 neural populations with increasing numbers of neurons. Neurons were
1250 arranged by the weighting value on the first dimension of the cue epoch
1251 (left) or the reward epoch (right). Values were normalized to the
1252 discriminability by the full population. Lines and shaded areas represent
1253 mean and 95th percentile range, respectively. Dotted lines indicate increase
1254 expected by random incorporation of the neurons. (**g**) Temporal shifts in

representational geometry. The same shuffled data as in d was shown here. We considered the baseline-epoch responses to be chance level. (**h**) Relationship between temporal coherence and dynamics of the PRC population responses (Methods). Vertical axis indicates proportion of the task representations sustained between different epochs, and horizontal axis indicates the degree of temporal shifts. Each single point corresponds to the population response in a subset of trials. The discriminability by the cue-epoch and reward-epoch responses is shown as blue points. The same for the baseline-epoch responses and shuffled responses are shown as deep gray and light gray points, respectively. In box plots, the same convention as in Fig. 4.